JACS
JOURNAL OF THE AMERICAN CHEMICAL SOCIETY

Communication

pubs.acs.org/JACS

Energy Storage during Compression of Metal–Organic Frameworks

Yu-Run Miao, Zhi Su,[†] and Kenneth S. Suslick*

Department of Chemistry, University of Illinois at Urbana–Champaign, Urbana, Illinois 61801, United States

Supporting Information

ABSTRACT: Practical applications of metal–organic framework (MOF) materials require an in-depth understanding of their mechanical properties. We have investigated the mechanical properties and energy absorption behavior of single crystals of four isostructural UiO-type MOFs under uniaxial compression. In situ nanocompression experiments were used to measure the mechanical behavior of individual MOF nanocrystals under compression within a transmission electron microscope. The plasticity and endothermicity during deformation of MOFs shows a surprising potential for absorption and dissipation of mechanical shock. At compressive stress below 2 GPa, relatively small amounts of energy (<0.3 kJ/g) are absorbed by the compression of these MOFs. As the stress was increased, however, the energy absorption was significantly enhanced. Above 2 GPa, the energy absorption typically reaches 3–4 kJ/g; for comparison, the energy release in the explosion of TNT is ∼4 kJ/g. Gram for gram, MOFs can absorb as much energy as a high explosive can release.

Metal–organic frameworks (MOFs) have been extensively studied over the past decade for potential applications in gas storage, separation, and catalysis.[1] Recently, there is a growing interest in the mechanical properties of MOFs and their related structural changes under pressure,[2] and such studies are primarily carried out using nanoindentation[3] and diamond anvil cell[4] (DAC) techniques. Relatively little exploration of MOFs' bulk mechanical properties, however, has been reported under compressive stress beyond the elastic limits, which is essential to evaluate their mechanochemical behavior. Furthermore, the accompanying energy absorption during the structural transition of MOFs under compressive stress is an interesting phenomenon that might prove useful for a new generation of mechanical energy absorbing materials.[5] Recent developments in impact mitigating macro and microstructural architectures and composites[6] emphasize the need for a fundamental understanding of the mechanical properties of their components, including elastic modulus, yield strength and load-capacity, especially under extreme conditions (such as shockwave pressures).[7] The possibility of extending impact mitigation to nanostructured materials motivated us to investigate the mechanical and energetic properties of MOFs at high compressive stress where densification is likely to occur.

Among the various MOF structures reported to date, the isoreticular UiO MOFs are highly attractive due to their chemical stability and synthetic versatility.[8] The UiO MOFs consist of $Zr_6O_4(OH)_4$ clusters interconnected by rigid dicarboxylate ligands, whose size and chemical functionality can be readily tuned (Figure 1). The high framework connectivity (each $Zr_6O_4(OH)_4$ cluster is linked to 12 other clusters) makes UiO MOFs very stable and capable of retaining porosity even after removal of solvates.[9]

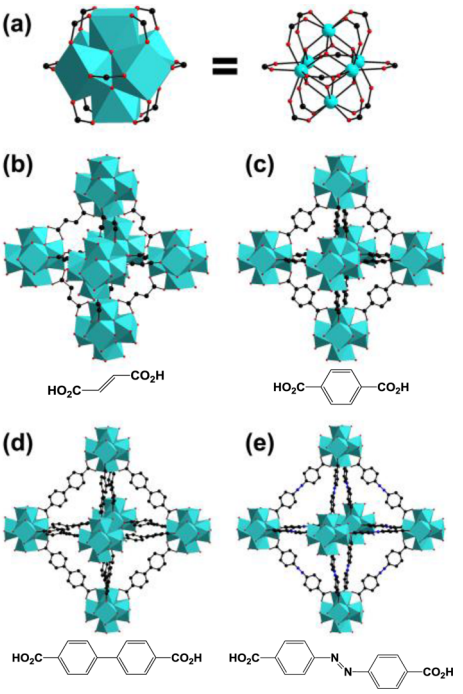

Figure 1. Crystal structures of (a) the $Zr_6O_4(OH)_4$ cluster and UiO-MOFs: (b) MOF-801, (c) UiO-66, (d) UiO-67 and (e) UiO-abdc, with the corresponding dicarboxylic acid precursors below each structure. Zr, turquoise; C, black; O, red; N, blue. H omitted for clarity.

We have previously shown that an in situ compression experiment inside a transmission electron microscope (TEM) is a useful tool in visualizing the compression-induced deformation of individual ZIF-8 microcrystals.[2d] Here, we report our study on the plastic deformation of isostructural UiO MOFs using in situ compression. Specifically, we synthesized nanocrystals of four UiO MOFs:[8] MOF-801 [$Zr_6O_4(OH)_4(fumarate)_6$], UiO-66 [$Zr_6O_4(OH)_4(terephthalate)_6$], UiO-67 [$Zr_6O_4(OH)_4(bpdc)_6$] (bpdc: 4,4′-biphenyl dicarboxylate), and UiO-abdc [$Zr_6O_4(OH)_4(abdc)_6$] (abdc: 4,4′-azobenzene dicarboxylate) (Figure 1). Their mechanical behavior was measured by recording the load–displacement curve of individual MOF crystals during

Received: February 14, 2017

DOI: 10.1021/jacs.7b01593
J. Am. Chem. Soc. XXXX, XXX, XXX–XXX

uniaxial compression with a flat-punch inside a TEM. We find that the elastic modulus and mechanical energy absorption of UiO MOFs are strongly dependent on the maximum applied pressure, which provides insights into the complex mechanical behavior of MOFs and their potential applications under extreme conditions.

Nanocrystals of MOF-801, UiO-66, UiO-67, and UiO-abdc were prepared via acid modulated solvothermal synthesis based on previous reports[10] with modification, desolvated, and their porosity measured (Supporting Information, Table S1, Figure S1). Powder X-ray diffraction (PXRD) confirms that all MOFs are crystalline and match well with their respective simulated patterns (SI, Figure S2). As shown by the scanning electron microscopy (SEM) images in Figure 2, the MOF nanocrystals exhibit well-defined octahedral morphology with narrow size distribution, from approximately 300 nm for MOF-801 to 500 nm for UiO-abdc.

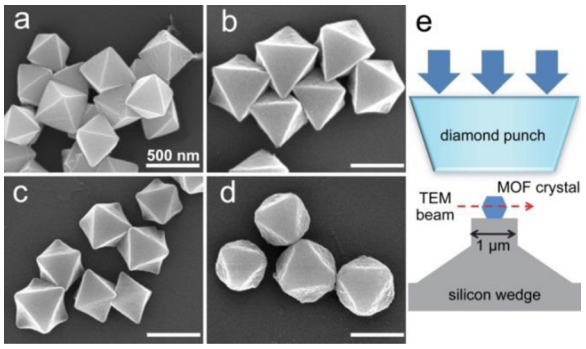

Figure 2. SEM images of (a) MOF-801, (b) UiO-66, (c) UiO-67, and (d) UiO-abdc; all scale bars indicate 500 nm. (e) Schematic of the nanocompression apparatus.

For the in situ TEM compression, the desolvated MOF nanocrystals were dispersed on a silicon holder with a 1-μm wide flat surface. A 2-μm flat diamond punch compressed perpendicularly to the (111) facet of the crystals at 1 nm/s. The nanocrystal octahedron geometry ensures that their top and bottom facets are parallel to the silicon substrate and diamond punch plane regardless of their in-plane orientation, which is prerequisite for uniaxial compression; images of the crystals viewed top down before and after compression are shown in Figure 3 and SI Figure S3. The dimensions and morphology of the crystals were recorded during compression using TEM, simultaneously with the load–displacement data collected from the nanocompression; the mechanical parameters (strain, stress, and elastic modulus) were then calculated from the analysis of the load–displacement curves and TEM images (SI Figure S4). During the compression, the MOF nanocrystals were gradually deformed, with no abrupt cracking or fracturing observed, as shown in the smoothness of the load–displacement curves (Figure 3). In the unloading stage after the compression, the punch retracts from the crystal and the crystal rebounds slightly.

Young's modulus (the slope of a stress–strain curve) is a characteristic parameter that measures the stiffness of a material and includes both elastic and inelastic components. To compare the stiffmess of all the MOFs, we calculated their effective Young's modulus during loading (E_{load}) by linearly fitting the stress–strain between 0.2 and 0.4 strain (Figure 4). The effective modulus is highest in UiO-66 (7.8 GPa), and decreases to 5.1 for UiO-67 and 3.9 GPa for UiO-abdc as the linkers are further extended. Previous computational studies predict a decreasing trend in the shear and

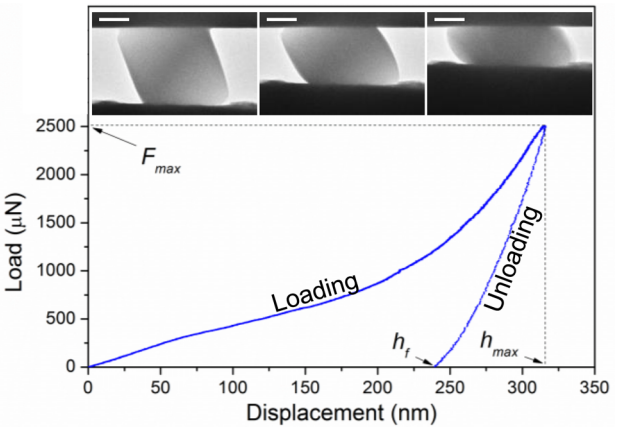

Figure 3. Cross-sectional TEMs of a UiO-66 single crystal during compression (inset, scale bars 100 nm) and the resulting load–displacement curve showing the load (F_{max}) and displacement (h_{max}) at maximum compression and the final displacement (h_f). The nanocrystal octahedrons ensure that their top and bottom facets are parallel to the silicon "anvil" substrate and diamond punch planes regardless of their in-plane orientation. The deformation of the MOF crystals during pore collapse is severe and the material "pancakes" during compression.

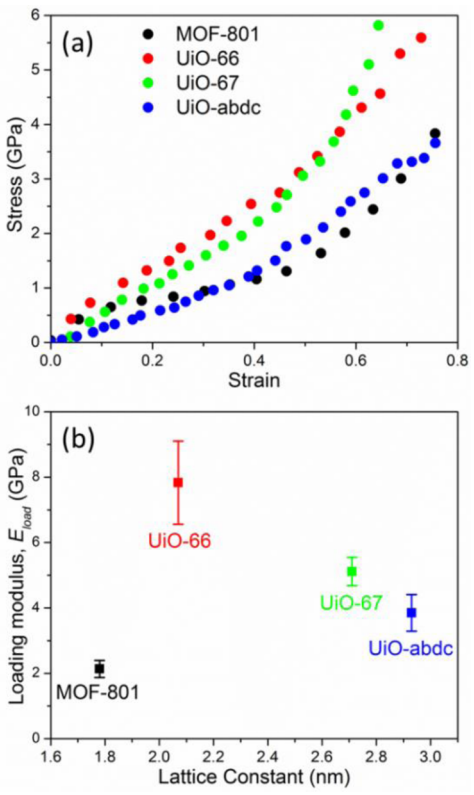

Figure 4. (a) Representative stress–strain plot and (b) loading modulus E_{load} (b) for UiO MOFs.

bulk moduli of UiO MOF structure as the linker length increases.[11] MOF-801, however, has the lowest modulus of 2.1 GPa even though its fumarate linker is the shortest among the series: this abnormally low compressive modulus of MOF-801 prompted us to investigate structural defects as a probable cause.

It is known that UiO MOFs synthesized with acid modulators may contain missing-linker type defects,[12] in which a dicarboxylate linker is replaced by two monodentate modulators, thus reducing the framework connectivity. To determine the defect

DOI: 10.1021/jacs.7b01593
J. Am. Chem. Soc. XXXX, XXX, XXX–XXX

concentration quantitatively, we digested the desolvated MOFs in H_2SO_4/DMSO-d_6 solution, and analyzed the relative amount of dicarboxylate ligand and monocarboxylate modulator in ^{1}H NMR spectrum (SI Figure S5, Table S2).[13] Although the modulator concentration relative to the dicarboxylate ligand is below 5% in UiO-66, UiO-67, and UiO-abdc (all of which are synthesized using acetic acid as modulator), MOF-801 is prepared using formic acid as modulator and it has a much higher defect concentration: 18% relative to the fumarate ligand. It is noteworthy that deviation of the experimental elemental analysis from theoretical values was also seen in previous synthesis of MOF-801,[8d] which probably originates from its high defect concentration. The weakening of UiO MOF structure due to such missing-linker defects is predicted in a recent computational study.[14] Furthermore, the smaller size of formate groups compared to acetate groups may also result in less steric hindrance and higher compressibility during deformation.

The unloading modulus E_{unload} is measured during the elastic recovery of the compressed, densified MOF structure and varies with the maximum stress applied to the nanocrystals before release (SI Figure S6). We measured E_{unload} of the MOF nanocrystals as a function of that applied maximum stress, as shown in Figure 5. As observed, the E_{unload} is essentially linear with

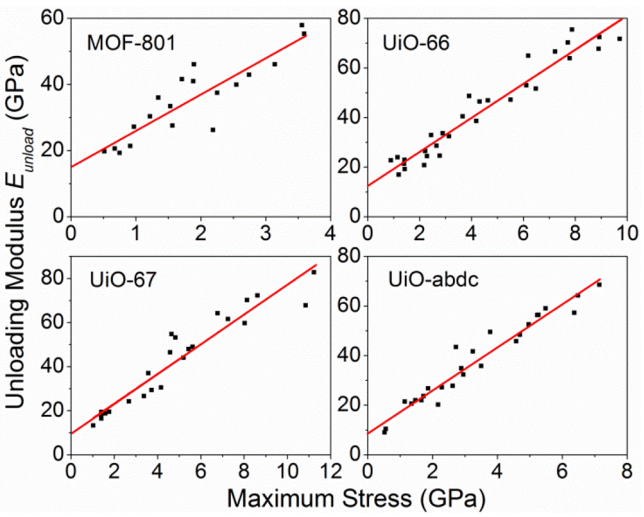

Figure 5. Unloading modulus (E_{unload}) of UiO MOFs as a function of applied stress with a linear fitting; the intercept gives E_0, which is the estimated elastic modulus of the intact, stress-free structure.

increasing maximum stress, and a linear fitting is given for the E_{unload}–stress relationship (SI Table S3). The intercept E_0, i.e., extrapolated E_{unload} with no pressure applied, is the estimated elastic modulus of the intact, stress-free structure. In contrast to the loading modulus (which includes both the elastic and inelastic contributions), E_0 (which is only the elastic component) decreases with increasing linker length: e.g., for MOF-801, E_0 = 15 GPa, and for UiO-abdc, E_0 = 9 GPa. The elastic recovery is therefore less influenced by defects in the structures of the MOFs.

The stiffening coefficient β, i.e., slope value from the linear fitting of E_{unload}–stress for the MOFs, is within the range for common inorganic materials.[15] The comparatively low value of E_0 for MOFs, however, leads to huge pressure-induced stiffening effects (i.e., β/E_0). For example, at an applied pressure of 10 GPa, the elastic modulus of silicon (i.e., its stiffness) increases by only 42%, whereas the MOFs are stiffened dramatically more: MOF-801 by 730%, UiO-66 by 560%, UiO-67 by 670%, UiO-abdc by 970%. This difference between MOFs and nonporous inorganic solids results from the pore collapse and densification in MOFs during compression, a deformation mechanism not available to dense materials.

The mechanical energy absorbed by individual MOF nanocrystals in a loading–unloading cycle can be calculated from the integration of the area under the load–displacement curve, which defines E_{max}, the maximum mechanical energy input, and E_f, the total energy absorbed during the loading–unloading cycle (SI Figure S7). To evaluate the performance of UiO MOFs as mechanical energy absorbers, we plotted E_f values as a function of maximum stress in Figure 6. At stresses below 2 GPa, relatively

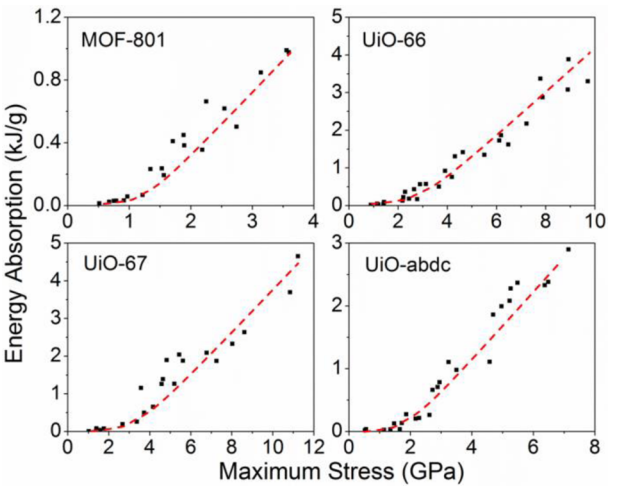

Figure 6. Mechanical energy absorption of UiO MOFs as a function of stress. The red dashed curves are provided as guides to the eye.

small amounts of energy (<0.3 kJ/g) are absorbed by MOFs. As the stress is increased, however, the energy absorption is significantly enhanced, possibly from the endothermic bond breakage in the structure. This is less true for MOF-801, which collapses fully at only 3.5 GPa.

At high applied pressures (>8 GPa), the energy absorption E_f generally reaches up to 3–4 kJ/g for the MOFs under our experimental conditions. For comparison, the energy released in an explosion of TNT is ~4 kJ/g. Gram for gram, MOFs can absorb as much energy as a high explosive can release. The highest previous energy storage reported was only 60 J/g, but this was measured for bulk powder of a MOF (MIL-53) only at low applied pressures (≤110 MPa) and utilized only reversible structural transitions.[5c]

Energy absorption during compression of bulk MOF materials may include contributions from normal strain, shear strain, powder packing, as well as pore volume collapse. Because only normal strain and volume collapse are measured in our single-crystal experiments, our results present a lower-bound estimate of the energy absorption capacity of MOFs.

An efficient energy absorber should maintain a high capacity relative to the energy input across a broad range of stress. To evaluate the efficiency of MOFs, we calculated an energy absorption ratio A, defined as $A = E_f/E_{max}$ (SI Figure S8). The maximum mechanical energy E_{max} has contributions from both elastic and plastic deformation, whereas the final energy absorption E_f contains only the plastic deformation. One may expect the deformation to be mostly elastic as the applied maximum stress approaches zero, and this seems to be the case with low values of A observed at low applied pressures. As the

DOI: 10.1021/jacs.7b01593
J. Am. Chem. Soc. XXXX, XXX, XXX–XXX

maximum stress is increased, A increases rapidly and flattens above ~2 GPa. Although the absolute value of energy absorption E_f increased steadily above 2 GPa, the ratio A is maintained at about 80% for all the UiO MOFs, up to the highest pressures applied during our experiments. This provides some confidence that the high plasticity and endothermicity of structural deformations will prove useful for energy absorption by MOFs over a wide range of applied stress.

For comparison, we contrast the mechanical behavior of MOFs to ceramic materials. Nanocompression experiments were performed on ~500 nm octahedral nanocrystals of Cu_2O prepared as reported[16] (SI Figure S9). A nanocrystal of Cu_2O was compressed consecutively at increasing applied pressures to reveal the evolution of its mechanical behavior (SI Figure S10). Although the deformation in the first compression is highly elastic, the energy-absorbing hysteresis becomes obvious in the second cycle as the maximum pressure rises. Further increasing the load in the third cycle leads to yielding beyond the elastic limit and discontinuity events, with the development of banding due to local stress in the nanoparticle as can be seen from the in situ TEM images (SI Figure S11). The energy absorption in the nanoparticle is only 59 J/g even when completely flattened, as compared to the multi kJ/g scale in MOF at similar strains (SI Table S4). Likewise, compression experiments on CeO_2 nanoparticles (SI Figure S12) show similar behavior and ductile deformation with very low energy absorption. These comparisons emphasize the unique mechanical behavior of MOFs.

In conclusion, we have measured the mechanical behavior of individual UiO MOF nanocrystals under compression in situ during transmission electron microscopy. We have observed that the elastic modulus and mechanical energy absorption of UiO MOF single crystals are strongly dependent on the applied pressure, which provides insights into the relationship between structure and mechanical properties of MOF materials. Furthermore, the mechanochemical behavior of MOFS (their plasticity, densification, and endothermicity during deformation and collapse) suggests potential for absorption and dissipation of mechanical shock.

■ ASSOCIATED CONTENT

Supporting Information

The Supporting Information is available free of charge on the ACS Publications website at DOI: 10.1021/jacs.7b01593.

Experimental details and instrumentation, PXRD, N_2 adsorption isotherms, TEM images (PDF)

Video showing compression of a UiO-66 nanocrystal (AVI)

■ AUTHOR INFORMATION

Corresponding Author

*ksuslick@illinois.edu

ORCID

Kenneth S. Suslick: 0000-0001-5422-0701

Present Address

†School of Chemistry and Materials Science, Nanjing Normal University, Nanjing, 210023 Jiangsu, P. R. China.

Notes

The authors declare no competing financial interest.

■ ACKNOWLEDGMENTS

Funding from the U.S. Navy (MURI N000141210828).

■ REFERENCES

(1) (a) Furukawa, H.; Cordova, K. E.; O'Keeffe, M.; Yaghi, O. M. *Science* **2013**, *341*, 1230444. (b) Liu, J. W.; Chen, L. F.; Cui, H.; Zhang, J. Y.; Zhang, L.; Su, C. Y. *Chem. Soc. Rev.* **2014**, *43*, 6011. (c) Mondloch, J. E.; Katz, M. J.; Isley Iii, W. C.; Ghosh, P.; Liao, P.; Bury, W.; Wagner, G. W.; Hall, M. G.; DeCoste, J. B.; Peterson, G. W.; Snurr, R. Q.; Cramer, C. J.; Hupp, J. T.; Farha, O. K. *Nat. Mater.* **2015**, *14*, 512. (d) Suslick, K. S.; Bhyrappa, P.; Chou, J. H.; Kosal, M. E.; Nakagaki, S.; Smithenry, D. W.; Wilson, S. R. *Acc. Chem. Res.* **2005**, *38*, 283.

(2) (a) Tan, J. C.; Cheetham, A. K. *Chem. Soc. Rev.* **2011**, *40*, 1059. (b) Yang, K.; Zhou, G.; Xu, Q. *RSC Adv.* **2016**, *6*, 37506. (c) Coudert, F.-X. *Chem. Mater.* **2015**, *27*, 1905. (d) Su, Z.; Miao, Y.-R.; Mao, S.-M.; Zhang, G.-H.; Dillon, S.; Miller, J. T.; Suslick, K. S. *J. Am. Chem. Soc.* **2015**, *137*, 1750.

(3) (a) Moggach, S. A.; Bennett, T. D.; Cheetham, A. K. *Angew. Chem.* **2009**, *121*, 7221. (b) Li, W.; Thirumurugan, A.; Barton, P. T.; Lin, Z.; Henke, S.; Yeung, H. H.-M.; Wharmby, M. T.; Bithell, E. G.; Howard, C. J.; Cheetham, A. K. *J. Am. Chem. Soc.* **2014**, *136*, 7801.

(4) (a) Chapman, K. W.; Halder, G. J.; Chupas, P. J. *J. Am. Chem. Soc.* **2009**, *131*, 17546. (b) Gagnon, K. J.; Beavers, C. M.; Clearfield, A. *J. Am. Chem. Soc.* **2013**, *135*, 1252. (c) Hobday, C. L.; Marshall, R. J.; Murphie, C. F.; Sotelo, J.; Richards, T.; Allan, D. R.; Duren, T.; Coudert, F. X.; Forgan, R. S.; Morrison, C. A.; Moggach, S. A.; Bennett, T. D. *Angew. Chem., Int. Ed.* **2016**, *55*, 2401.

(5) (a) Yot, P. G.; Boudene, Z.; Macia, J.; Granier, D.; Vanduyfhuys, L.; Verstraelen, T.; Van Speybroeck, V.; Devic, T.; Serre, C.; Ferey, G.; Stock, N.; Maurin, G. *Chem. Commun.* **2014**, *50*, 9462. (b) Banlusan, K.; Strachan, A. *J. Phys. Chem. C* **2016**, *120*, 12463. (c) Yot, P. G.; Vanduyfhuys, L.; Alvarez, E.; Rodriguez, J.; Itié, J.-P.; Fabry, P.; Guillou, N.; Devic, T.; Beurroies, I.; Llewellyn, P. L.; et al. *Chem. Sci.* **2016**, *7*, 446. (d) Banlusan, K.; Antillon, E.; Strachan, A. *J. Phys. Chem. C* **2015**, *119*, 25845.

(6) (a) Gibson, L. J.; Ashby, M. F. In *Cellular Solids: Structure and Properties*; Cambridge University Press: Cambridge, 1997; p 309. (b) Duoss, E. B.; Weisgraber, T. H.; Hearon, K.; Zhu, C.; Small, W.; Metz, T. R.; Vericella, J. J.; Barth, H. D.; Kuntz, J. D.; Maxwell, R. S.; Spadaccini, C. M.; Wilson, T. S. *Adv. Funct. Mater.* **2014**, *24*, 4905.

(7) Qiao, P.; Yang, M.; Bobaru, F. *J. Aerosp. Eng.* **2008**, *21*, 235.

(8) (a) Cavka, J. H.; Jakobsen, S.; Olsbye, U.; Guillou, N.; Lamberti, C.; Bordiga, S.; Lillerud, K. P. *J. Am. Chem. Soc.* **2008**, *130*, 13850. (b) Schaate, A.; Dühnen, S.; Platz, G.; Lilienthal, S.; Schneider, A. M.; Behrens, P. *Eur. J. Inorg. Chem.* **2012**, *2012*, 790. (c) Wißmann, G.; Schaate, A.; Lilienthal, S.; Bremer, I.; Schneider, A. M.; Behrens, P. *Microporous Mesoporous Mater.* **2012**, *152*, 64. (d) Furukawa, H.; Gándara, F.; Zhang, Y.-B.; Jiang, J.; Queen, W. L.; Hudson, M. R.; Yaghi, O. M. *J. Am. Chem. Soc.* **2014**, *136*, 4369.

(9) (a) Oien-Odegaard, S.; Bouchevreau, B.; Hylland, K.; Wu, L. P.; Blom, R.; Grande, C.; Olsbye, U.; Tilset, M.; Lillerud, K. P. *Inorg. Chem.* **2016**, *55*, 1986. (b) Zhang, T.; Manna, K.; Lin, W. *J. Am. Chem. Soc.* **2016**, *138*, 3241.

(10) Schaate, A.; Roy, P.; Godt, A.; Lippke, J.; Waltz, F.; Wiebcke, M.; Behrens, P. *Chem. - Eur. J.* **2011**, *17*, 6643.

(11) (a) Wu, H.; Yildirim, T.; Zhou, W. *J. Phys. Chem. Lett.* **2013**, *4*, 925. (b) Yang, L.-M.; Ganz, E.; Svelle, S.; Tilset, M. *J. Mater. Chem. C* **2014**, *2*, 7111.

(12) (a) Wu, H.; Chua, Y. S.; Krungleviciute, V.; Tyagi, M.; Chen, P.; Yildirim, T.; Zhou, W. *J. Am. Chem. Soc.* **2013**, *135*, 10525. (b) Cliffe, M. J.; Wan, W.; Zou, X.; Chater, P. A.; Kleppe, A. K.; Tucker, M. G.; Wilhelm, H.; Funnell, N. P.; Coudert, F.-X.; Goodwin, A. L. *Nat. Commun.* **2014**, *5*, 4176.

(13) Gutov, O. V.; Hevia, M. G.; Escudero-Adán, E. C.; Shafir, A. *Inorg. Chem.* **2015**, *54*, 8396.

(14) Thornton, A. W.; Babarao, R.; Jain, A.; Trousselet, F.; Coudert, F. X. *Dalton Trans.* **2016**, *45*, 4352.

(15) Mook, W. M.; Nowak, J. D.; Perrey, C. R.; Carter, C. B.; Mukherjee, R.; Girshick, S. L.; McMurry, P. H.; Gerberich, W. W. *Phys. Rev. B: Condens. Matter Mater. Phys.* **2007**, *75*, 214112.

(16) Ye, S.; Rathmell, A. R.; Ha, Y. C.; Wilson, A. R.; Wiley, B. J. *Small* **2014**, *10*, 1771.

DOI: 10.1021/jacs.7b01593
J. Am. Chem. Soc. XXXX, XXX, XXX−XXX